

Normal modes of a rectangular tank with corrugated bottom

LOUIS N. HOWARD¹ AND JIE YU^{2†}

¹Department of Mathematics, Massachusetts Institute of Technology, Cambridge, MA 02139, USA

²School of Mechanical, Aerospace and Civil Engineering, The University of Manchester, Manchester M60 1QD, UK

(Received 26 January 2007 and in revised form 9 August 2007)

We study some effects of regular bottom corrugations on water waves in a long rectangular tank with vertical endwalls and open top. In particular, we consider motions which are normal modes of oscillation in such a tank. Attention is focused on the modes whose internodal spacing, in the absence of corrugations, would be near the wavelength of the corrugations. In these cases, the perturbation of the eigenfunctions (though not of their frequencies) can be significant, e.g. the amplitude of the eigenfunction can be greater by a factor of ten or more near one end of the tank than at the other end. This is due to a cooperative effect of the corrugations, called Bragg resonance. We first study these effects using an asymptotic theory, which assumes that the bottom corrugations are of small amplitude and that the motions are slowly varying everywhere. We then present an exact theory, utilizing continued fractions. This allows us to deal with the rapidly varying components of the flow. The exact theory confirms the essential correctness of the asymptotic results for the slowly varying aspects of the motions. The rapidly varying parts (evanescent waves) are, however, needed to satisfy accurately the true boundary conditions, hence of importance to the flow near the endwalls.

1. Introduction

It has been recognized for well over twenty years that a series of corrugations on the bottom of a layer of water of otherwise uniform depth can have a cooperative effect on an incident water wave, if the latter has a wavelength close to twice the spacing of the corrugations. This phenomenon is usually referred to as ‘Bragg reflection’, ‘Bragg scattering’, or sometimes ‘Bragg resonance’, from its analogy to the similar effect with X-rays in crystals, which was discovered by the Braggs. While the water wave analogue may not have the fundamental scientific significance of the X-ray prototype, it does have some interesting features which have attracted studies of several kinds. For instance, while not especially common, there are some beaches which have a sizable number (ten or more) of shore parallel sandbars, with a nearly regular spacing comparable to half the wavelength of some ocean surface waves. There is some theoretical evidence that for these beaches the Bragg reflection effect may play a part not only in the response of the nearshore wave structure to incident waves from the

† Present address: Department of Civil, Construction and Environmental Engineering, North Carolina State University, Raleigh, NC 27695-7908, USA.

deep sea, but also in the formation and evolution of these parallel sandbar patches themselves (see, for instance, Mei, Hara, & Yu 2001; Yu & Mei 2000b).

The basic physical idea, as well as the first theoretical studies (which showed how a wavetrain of the appropriate frequency passing over a patch of sandbars would be partially reflected and so would have its amplitude reduced on leaving the patch) led to suggestions that perhaps artificial sandbars could be used to protect beaches. One might well question the practicality of this idea, simply on the grounds that real ocean wave fields are variable in frequency (and direction) and have a considerable random component. Nevertheless at least one attempt to try this on an actual beach has been made (Baillard *et al.* 1990;† see also Baillard, DeVries & Kirby 1992). A somewhat less obvious theoretical reason to question the protective effect of a series of bars, even with a nearly monochromatic and long-lasting wave field provided by a remarkably cooperative ocean, was put forward by Yu & Mei (2000a), where it was shown that under certain conditions a bar patch can actually *enhance* the wave amplitude onshore. This occurs when there is significant ordinary reflection from the shoreline, in addition to the Bragg reflection. The wave reflected from the shore also passes over the bar patch and is itself Bragg-reflected, producing a wave propagating back toward the shore which adds to the part of the original incident wave which has passed over the bar patch. If these two waves are in phase, they tend to enhance the wave field onshore. Whether or not this happens depends delicately on where the (effective) position of the shoreline reflector is with respect to the bar crests (Yu & Mei 2000a). The mathematics was provided by Mei (1985), who formulated an asymptotic theory based on the general ideas of slowly varying waves. This is appropriate here because the effect on a wavetrain of an individual bottom corrugation is generally quite small; it is only when the wavetrain passes over a number of bars with appropriate spacing that their collective effect can be more significant.

The present paper was largely motivated by the above-mentioned somewhat subtle interaction between the Bragg reflection of a series of sandbars and a shoreline reflection, particularly when the latter is strong, as for instance with a seawall. We decided to investigate the effects of a considerable number of bottom corrugations on the linear normal modes of a long rectangular tank with vertical ends. The water depth is otherwise uniform. We anticipated that the modes with natural frequencies close to the Bragg resonance frequency of the corrugations would be significantly affected. Since we want to have a large number of corrugations in the tank these would be relatively ‘high’ modes. For these modes, we expected a major perturbation on the eigenfunctions (not their natural frequencies), one which might well depend sensitively on the position of the endwalls with respect to the corrugation crests. This problem is treated using the asymptotic theory in §2.

The asymptotic theory of waves over a corrugated bottom describes the motion (in lowest approximation) locally as a superposition of two oppositely directed plane waves, but the amplitudes of these two waves vary slowly (in space and in time) in accordance with Mei’s equations. If one tries to go beyond the lowest approximation, however, it is generally not possible to satisfy the boundary conditions by using only these two waves, as they no longer have exactly the same functional form along a vertical wall. The asymptotic theory really satisfies these boundary conditions only in some kind of averaged sense. However, not all aspects of the flow are slowly varying,

† It was unsuccessful, mainly for a different practical reason: erosive processes caused the concrete ‘bars’ to sink rapidly into the underlying sand.

meaning that the asymptotic theory can suffer difficulties. This was indeed noticed in Yu & Mei (2000*b*), where the slow variation breaks down, causing difficulty in satisfying the boundary condition for sediment flux at higher order.

These motivate us to reconsider this normal mode problem, without making use of any slowly varying assumption. It will be recalled that for a flat bottom the linear wave problem has, for any given frequency, a family of two propagating waves going in opposite directions, and two infinite sets of evanescent waves decaying exponentially in opposite directions. To solve the normal mode problem for a tank with a flat bottom, it is only necessary to superpose the two propagating waves. By satisfying the boundary condition on both ends, the natural frequencies and their eigenfunctions can be determined, usually described as standing waves. The evanescent waves are not needed at all, and in fact are usually not even mentioned in elementary treatments. These solutions are, however, essential in problems with some other boundary conditions on the ends, for instance the wavemaker problem. The evanescent waves are also needed to solve the normal mode problem for a tank of uniform depth but with non-vertical endwalls. Thus, they can be of importance to problems concerning sediment erosion near to coastal structures.

We have found it possible to find analogues of both the two propagating waves and of the two families of evanescent waves for the corrugated bottom case. In doing this we have selected, mostly to simplify the mathematics, a specific form of bottom corrugations which is nearly sinusoidal at small amplitude but distinctly not so at high amplitude. This is described in §3, with details of some of the results in §4. Finally, in §5 we return to the normal mode problem, making use of these analogues of both the propagating and evanescent waves to deal more satisfactorily with the boundary conditions on the ends, as well as to improve some details of the surface elevation close to the ends. Concluding remarks follow in §6.

2. Asymptotic theory

The asymptotic theory of Bragg resonance of water waves (Mei 1985) assumes that both motions and sinusoidal bottom corrugations are of small amplitude. In the vertical plane (x, z) , where x is along the tank and z points upward with $z=0$ at the undisturbed water surface, the corrugated bottom with a wavenumber $2k_B$ is given by

$$z = -h + \epsilon h \cos 2k_B x, \quad (2.1)$$

where $\epsilon \ll 1$, and h is the mean (constant) water depth. Given the free surface $z = \zeta$, where

$$\zeta = \frac{1}{2}(Ae^{ik_B x} + Be^{-ik_B x})e^{-i\omega_B t} + \text{c.c.}, \quad (2.2)$$

the velocity potential, to the lowest-order approximation, can be described by

$$\phi = \frac{-ig}{2\omega_B} \frac{\cosh k_B(z+h)}{\cosh k_B h} (Ae^{ik_B x} + Be^{-ik_B x})e^{-i\omega_B t} + \text{c.c.}, \quad (2.3)$$

where the wave frequency ω_B is defined as

$$\omega_B^2 = gk_B \tanh k_B h. \quad (2.4)$$

A and B are the amplitudes of the two waves in opposite directions, slowly varying over the corrugations according to Mei's equations, i.e.

$$(\partial_t + C_g \partial_x)A = -i\Omega_c B, \quad (\partial_t - C_g \partial_x)B = -i\Omega_c A, \quad (2.5a, b)$$

where $C_g = \partial\omega_B/\partial k_B$ is the wave group velocity and

$$\Omega_c = \frac{1}{2}(\omega_B k_B h / \sinh 2k_B h) \epsilon \quad (2.6)$$

is the cutoff value of frequency deviation. If $\epsilon = 0$ (flat bottom), (2.2)–(2.6) give the exact solution to the linear wave problem in constant water depth, i.e. two waves propagating in opposite directions and with constant amplitudes A and B ; each of these waves has wavelength $2\pi/k_B$ which is twice the spacing of the corrugations that will be there when $\epsilon > 0$. Thus, defined by (2.4), ω_B is called the Bragg resonance frequency. The asymptotic theory (2.5) assumes that the spatial and time scales of A and B are both greater than the surface wavelength $2\pi/k_B$ and period $2\pi/\omega_B$, respectively, by a factor of $O(1/\epsilon)$. For example, in the case of waves passing over a patch of bottom corrugations, the length of the patch L and the time L/C_g are the appropriate slow scales. Mei also used ϵ to characterize the small wave slope, allowing for the inclusion of nonlinearity in the flow by considering higher-order terms.

For the normal mode problem in a tank of length L , the normal velocity must be zero at the vertical endwalls, i.e. at $x = x_0$ and $x = x_0 + L$. Note that $x = 0$ has been chosen as the location of a corrugation crest – see (2.1) – and the left endwall need not be at such a crest. Since $u = \partial\phi/\partial x$, we write from (2.3) that

$$A - e^{-i2\alpha} B = 0 \quad \text{at } x = x_0, \quad A - e^{-i2\beta} B = 0 \quad \text{at } x = L + x_0, \quad (2.7a, b)$$

where $\alpha = k_B x_0$, $\beta = k_B L - N\pi + \alpha$. We should like N to be the nearest integer number of corrugation wavelengths to the actual length of the tank. If L happens to be exactly half-way between two adjacent integer multiples of the corrugation wavelength, N is taken to be the larger of the two. To be definite, we shall also let $x = 0$ be the nearest corrugation crest to the left endwall at $x = x_0$. If the left endwall happens to be at a trough, we set $k_B x_0 = \pi/2$. In doing so, we thus set the ranges of α and β to be

$$-\pi/2 < \alpha \leq \pi/2, \quad -\pi/2 \leq \beta - \alpha < \pi/2, \quad (2.8)$$

which give a parallelogram in the (α, β) plane. The choice of N implies that the normal mode to be constructed will tend to the N th mode of the flat bottom case as $\epsilon \rightarrow 0$.

A wall is always an anti-node, meaning that the relative phase of the two surface waves (left- and right-going) is known and fixed. As α is a measure of the phase of the left endwall relative to the corrugation crests, it also provides a measure of the phase difference of the surface waves from the corrugation wave; β has a similar role for the right endwall. The critical importance of the phase relation among the three waves to the behaviour of Bragg scattering was pointed out in Yu & Mei (2000a). We shall see that both α and β are similarly critical for the spatial structure of some normal modes.

For $\epsilon > 0$, we look for time-periodic solutions, $A = \hat{A}(x)e^{-i\Omega t}$ and $B = \hat{B}(x)e^{-i\Omega t}$, which satisfy (2.5) and (2.7). This gives rise to eigenproblems, finding the eigenvalue Ω and the corresponding eigenfunctions $\hat{A}(x)$ and $\hat{B}(x)$. In the framework of the asymptotic theory, these periodic motions are normal modes of the tank with corrugated bottom. In view of (2.2), the frequency of the motion is $\omega = \omega_B + \Omega$. Depending on whether the detuning is subcritical ($\Omega^2 \leq \Omega_c^2$) or supercritical ($\Omega^2 > \Omega_c^2$), the wave amplitudes (i.e. the eigenfunctions) can vary either exponentially or oscillatorily along the tank.

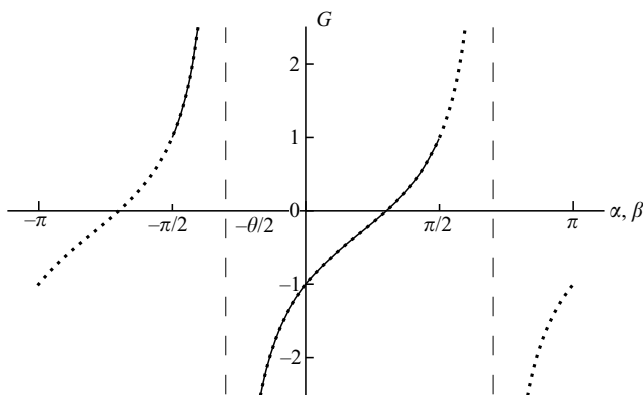


FIGURE 1. Graph of G as a function of its first argument (α or β) for some fixed value of $\theta/2$ (about 0.8 in this case). The vertical asymptotes (dashed lines) are at $-\theta/2$ and $\pi - \theta/2$. —, $G(\alpha, \theta/2)$; ·····, $G(\beta, \theta/2)$.

2.1. Exponential behaviour: $\Omega^2 < \Omega_c^2$

Define

$$Q = \sqrt{\Omega_c^2 - \Omega^2}, \quad q = QL/C_g. \tag{2.9}$$

$\widehat{A}(x)$ and $\widehat{B}(x)$ are linear combinations of $e^{qx/L}$ and $e^{-qx/L}$, so the wave amplitudes vary exponentially over the corrugations, as discussed in Mei (1985). For $\widehat{A}(x)$ and $\widehat{B}(x)$ to be non-trivial, the eigenvalues must satisfy

$$e^{-q} (1 - e^{i(\theta-2\alpha)}) (1 - e^{-i(\theta+2\beta)}) - e^q (1 - e^{-i(\theta+2\alpha)}) (1 - e^{i(\theta-2\beta)}) = 0, \tag{2.10}$$

where

$$\Omega/\Omega_c + iQ/\Omega_c \equiv e^{i\theta}, \quad 0 < \theta < \pi. \tag{2.11}$$

This range of θ is chosen since $Q > 0$ but Ω may have either sign. Since q is bounded by $\Omega_c L/C_g$, it is clear from (2.10) that if the coefficient of one of e^q or e^{-q} is zero, the other must be as well. When this is the case, we must have either $\alpha = \beta = \theta/2$ or $\alpha = \beta = -\theta/2$, in view of (2.8) and the fact that $q \neq 0$.† In the first case, the eigenvalue is given from (2.11) as $\Omega/\Omega_c = \cos 2\alpha$, and $Q/\Omega_c = \sin 2\alpha$; in the second case, $\Omega/\Omega_c = \cos(-2\alpha)$, and $Q/\Omega_c = \sin(-2\alpha)$. When neither of these is true, we can rewrite (2.10) as

$$e^{2q} = \frac{G(\alpha, \theta/2)}{G(\beta, \theta/2)}, \quad \text{where} \quad G(\alpha, \theta/2) \equiv \frac{\sin(\alpha - \theta/2)}{\sin(\alpha + \theta/2)}. \tag{2.12}$$

This determines the eigenvalue Ω , for given α , β and Ω_c . Figure 1 shows $G(\alpha, \theta/2)$ and $G(\beta, \theta/2)$ over the range of $[-\pi, \pi]$. Clearly, G is periodic of period π . Since $e^{2q} \geq 1$, there are only certain parts of the parallelogram (2.8) that can satisfy (2.12). These regions can be identified, with the assistance of figure 1, and are given as

† There are two other ways that the coefficients of e^q and e^{-q} in (2.10) could be zero, i.e. $e^{i\theta} = e^{i2\alpha} = e^{-i2\alpha}$, or $e^{i\theta} = e^{i2\beta} = e^{-i2\beta}$. It is easily seen that in both cases $e^{i2\theta} = 1$, requiring $\theta = 0$ or π and $Q = 0$ as well.

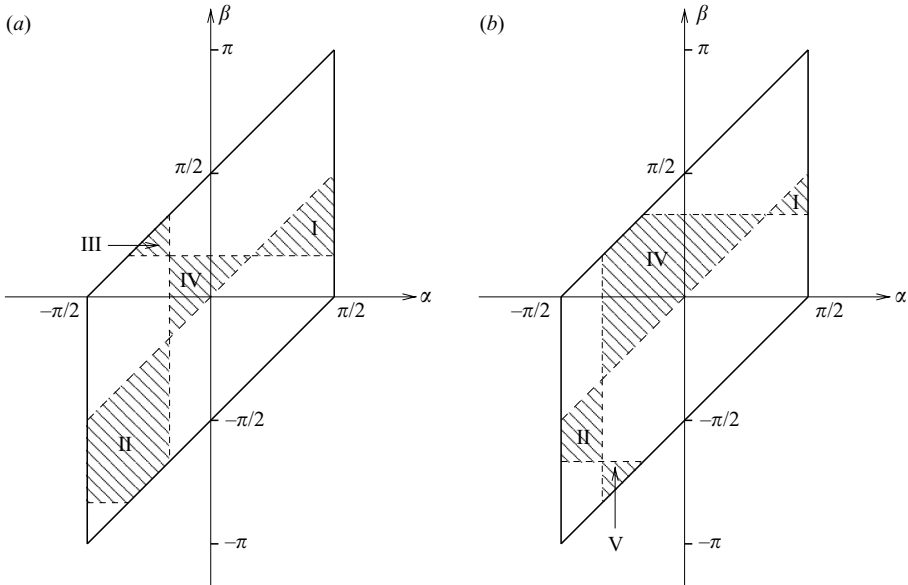


FIGURE 2. The possible values of α and β for normal modes of subcritical detuning conditions (exponential behaviour). (a) $\theta < \pi/2$; (b) $\theta > \pi/2$.

follows:

$$\left. \begin{aligned}
 \text{I} \quad & \frac{\theta}{2} < \beta < \alpha \leq \frac{\pi}{2}; \\
 \text{II} \quad & -\frac{\pi}{2} < \alpha < -\frac{\theta}{2}, \quad -\pi + \frac{\theta}{2} < \beta < \alpha < -\theta/2, \quad \text{and} \quad \beta - \alpha \geq -\frac{\pi}{2}; \\
 \text{III} \quad & -\frac{\pi}{2} < \alpha < -\frac{\theta}{2}, \quad \frac{\theta}{2} \leq \beta < \alpha + \frac{\pi}{2}; \\
 \text{IV} \quad & -\frac{\theta}{2} < \alpha < \beta < \frac{\theta}{2}, \quad \beta - \alpha < \frac{\pi}{2}; \\
 \text{V} \quad & -\frac{\theta}{2} < \alpha \leq \frac{\theta}{2}, \quad -\pi/2 + \alpha < \beta < -\pi + \frac{\theta}{2}.
 \end{aligned} \right\} \quad (2.13)$$

The location of these regions depends on the value of θ . In particular, if $\theta < \pi/2$, region V is empty, as is region III if $\theta > \pi/2$. Figures 2(a) and 2(b) show the sketches of these regions inside the parallelogram for small and large θ , respectively.

Given α and β , a convenient way to find Ω is as follows. We first select a sequence of values of θ , consistent with at least one of the regions in (2.13). For each θ , q is computed from (2.12). Since $QL/C_g = q$, it follows from (2.11) that $\Omega_c L/C_g = q/\sin \theta$ and $\Omega L/C_g = \cos \theta \Omega_c L/C_g$ (i.e. $\Omega = \cos \theta \Omega_c$). A correspondence is thus established between the chosen sequence of θ and a sequence of pairs of Ω and Ω_c , given the parameters α, β, h, L and ω_B specifying the problem. Note that with ω_B and h being given, Ω_c and ϵ play virtually the same role: cf. (2.6). Recall that ϵh is the amplitude of corrugations. It is worth noting that $\Omega L/C_g$ and $\Omega_c L/C_g$ are the dimensionless detuning and cutoff frequencies, respectively, since the slow time scale is L/C_g . Moreover, their relationship, given parametrically via θ , is solely determined by α and β : cf. (2.9)–(2.12). Thus, the procedure just outlined allows us to construct a graph of $\Omega L/C_g = f(\Omega_c L/C_g, \alpha, \beta)$, for which a subcritical normal mode exists.

Once the eigenvalue Ω is known, the eigenfunctions are found to be

$$\widehat{A}(x) = a [\sin(\alpha + \theta/2) e^{-i\theta} e^{q(x-x_0)/L} - \sin(\alpha - \theta/2) e^{-q(x-x_0)/L}], \quad (2.14a)$$

$$\widehat{B}(x) = a [\sin(\alpha + \theta/2) e^{q(x-x_0)/L} - \sin(\alpha - \theta/2) e^{-i\theta} e^{-q(x-x_0)/L}], \quad (2.14b)$$

where a is constant and arbitrary. From these, the actual surface elevation profile can be obtained from (2.2). The ratio of the surface amplitudes at the right and left end of the tank is given by

$$|\widehat{A}(x_0 + L)/\widehat{A}(x_0)| = [(\cos \theta - \cos 2\alpha)/(\cos \theta - \cos 2\beta)]^{1/2}. \quad (2.15)$$

Various examples will be presented later in comparison with the numerical results from the exact theory of §3. We cite one simple case here to illustrate the meaning of the exponential behaviour. This is a case of perfect tuning ($\Omega = 0$) when $\theta = \pi/2$. We take from region I in (2.13) $\alpha = 5\pi/12$ and $\beta = 4\pi/15$, i.e. the left endwall of the tank is $5/12$ and the right end $4/15$ of a wavelength to the right of the nearest crest. If $N = 16$, $k_B L = N\pi + \beta - \alpha = 15.85\pi$, i.e. the length of the tank is less than 16 corrugation wavelengths by about 1%. From (2.12), $q = 1.1997$. Since $Q = \Omega_c$, we have $\Omega_c L/C_g = q$. For $k_B h = 0.5$, we find from (2.6) that $\epsilon \simeq 0.1048$, and from (2.15) that $|\widehat{A}(x_0 + L)/\widehat{A}(x_0)| \simeq 2.878$. The frequency of the normal mode is exactly ω_B , comparing with $1.0087\omega_B$, which is the natural frequency of the 16th mode of the flat-bottomed tank. Thus, in the presence of bottom corrugations of amplitude only 0.1048 times the water depth, though the frequency is changed very little, the eigenfunction of this mode is altered significantly: the ‘standing wave’ is almost three times greater at the right end than at the left (in terms of energy density, it is $2.878^2 = 8.2829$ times). By a small shift of the relative position of the corrugations and the ends, keeping the tank length fixed, we could convert β into $-\alpha$ and α into $-\beta$, switching to region II, and find the wave amplitude greater in the same ratio at the left end.

2.2. Linear behaviour: $\Omega^2 = \Omega_c^2$

When the wave frequency deviates from ω_B by exactly $\pm\Omega_c$, \widehat{A} and \widehat{B} have a linear dependence in x , as in Mei (1985). The eigenvalue is found to be

$$\Omega L/C_g = \frac{1}{2}(\cot \beta - \cot \alpha), \quad -\Omega L/C_g = \frac{1}{2}(\tan \beta - \tan \alpha). \quad (2.16a, b)$$

Since $\Omega_c > 0$, the values of α and β satisfying (2.16) can only fall in the regions shown in figure 3(a) for $\theta = 0$ ($\Omega = \Omega_c$) and in figure 3(b) for $\theta = \pi$ ($\Omega = -\Omega_c$). Note that region III for $\theta = 0$ is a subset of region IV for $\theta = \pi$, and region V for $\theta = \pi$ is a subset of region II for $\theta = 0$. Therefore, given a pair of (α, β) in the two triangles of the parallelogram, $[-\pi/2 < \alpha < 0, 0 \leq \beta < \alpha + \pi/2]$ and $[-\pi/2 < \alpha < 0, -\pi/2 + \alpha < \beta < -\pi/2]$, both $\Omega = \Omega_c$ and $\Omega = -\Omega_c$ can occur. In the triangles, $[0 < \alpha < \pi/2, -\pi/2 + \alpha < \beta < 0]$ and $[0 < \alpha < \pi/2, \pi/2 < \beta < \pi/2 + \alpha]$, neither of (2.16) can be satisfied.

In the (Ω, Ω_c) plane, the region in which the amplitudes have exponential behaviour is $-\Omega_c < \Omega < \Omega_c$. This is a wedge opening upward, with vertex at the origin. Any mode which (for some $\Omega_c > 0$) lies inside this wedge has a frequency which deviates from ω_B by no more than $|\Omega_c|$, and must approach some normal mode of the flat-bottomed tank as $\epsilon \rightarrow 0$ (i.e. $\Omega_c \rightarrow 0$). The latter is a standing wave with wavenumber $k_n = n\pi/L$, where n is an integer, and frequency $\omega_n^2 = gk_n \tanh k_n h$. Since none of ω_n is necessarily exactly equal to ω_B , for sufficiently small ϵ there is usually no exponential mode at all. In other words, if there are any solutions of (2.11) and

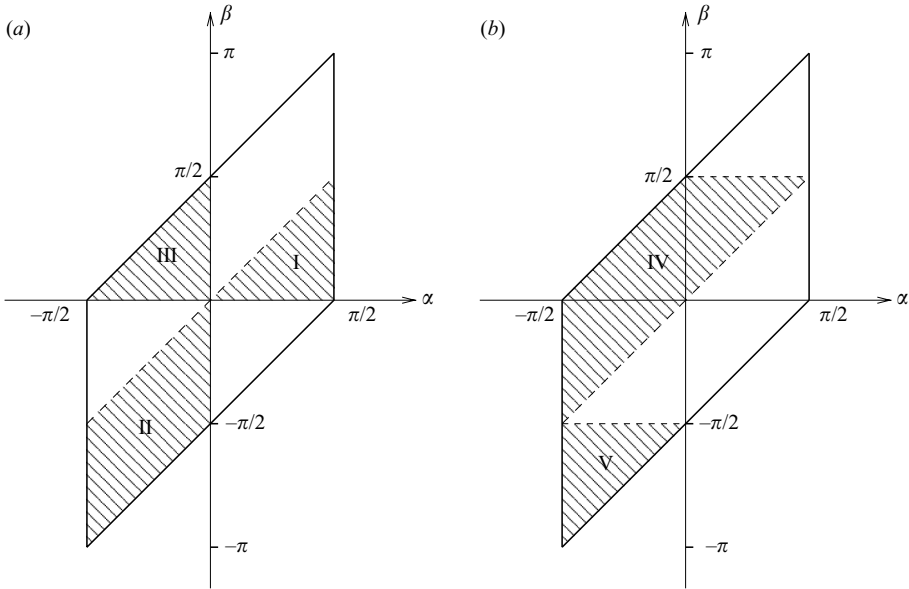


FIGURE 3. The possible values of α and β for normal modes of linear behaviour, i.e. detuned from the Bragg resonance frequency by exactly the cutoff value. (a) $\Omega = \Omega_c$ ($\theta = 0$); (b) $\Omega = -\Omega_c$ ($\theta = \pi$).

(2.12) for some $\epsilon > 0$, then as $\epsilon \rightarrow 0$ the corresponding Ω must eventually leave the wedge, passing through its boundary at one of the points given by (2.16a) or (2.16b). Outside the wedge, there are the normal modes (for some $\epsilon > 0$) whose amplitudes vary oscillatorily along the tank, as will be seen in §2.3. If ω_B happens to be a natural frequency of the flat-bottomed tank, the exponential case can occur only when $L = N\pi/k_B$, i.e. when $\alpha = \beta$. Both of (2.16) are satisfied with $\epsilon = 0$, but neither can be for any $\epsilon > 0$. In this case the N th mode of the flat-bottomed tank passes directly into the wedge of exponential behaviour as soon as ϵ becomes positive, and stays there. For $\alpha \neq \beta$, this N th mode must first become an oscillatory mode for sufficiently small ϵ , then enter the wedge, becoming an exponential mode at some positive value of ϵ . In some cases one of its neighbours may also enter the wedge for large enough ϵ , i.e. $(N+1)$ th or $(N-1)$ th mode. However, there never seem to be more than two modes inside the wedge, there being at most two possible entry points on its boundary. This is illustrated by an example in figure 4, using the asymptotic theory at $\alpha = -\pi/6$ and $\beta = \pi/6$, in which there are eventually two exponential modes. On the $(\Omega L/C_g, \Omega_c L/C_g)$ plane, it shows the tracks of the N th and $(N+1)$ th modes down to $\epsilon = 0$. The calculation inside the wedge is carried out using the procedure described above; for the outside, it is done as described in §2.3.

For the example in §2.1, $\Omega = \Omega_c = 0.0062731\omega_B$ from (2.16a), and $\Omega_c = 0.21273\epsilon\omega_B$ from (2.6). Thus, $\epsilon = 0.029488$ for the mode to be detuned by exactly the cutoff frequency.

2.3. Oscillatory behaviour: $\Omega^2 > \Omega_c^2$

This is the case of supercritical detuning, as classified in Mei (1985). Define

$$Q = \sqrt{\Omega^2 - \Omega_c^2}, \quad q = QL/C_g. \quad (2.17)$$

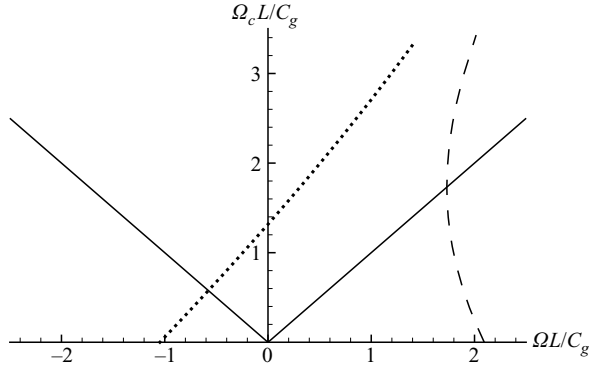


FIGURE 4. The two modes enter the wedge at some $\epsilon > 0$, becoming exponential modes, for $\alpha = -\pi/6$ and $\beta = \pi/6$. $\cdots\cdots$, N th mode; $-\cdots-$, $(N+1)$ th mode.

\hat{A} and \hat{B} are linear combinations of $e^{iqx/L}$ and $e^{-iqx/L}$, and thus oscillate (slowly) along the tank. For non-trivial solutions, we require

$$e^{iq}(1 - e^{-i2\beta} T^{-1})(1 - e^{-i2\alpha} T) - e^{-iq}(1 - e^{-i2\beta} T)(1 - e^{-i2\alpha} T^{-1}) = 0, \quad (2.18)$$

where $T = \Omega/\Omega_c + Q/\Omega_c$. It is readily seen from (2.17) that

$$\Omega/\Omega_c = \frac{1}{2}(T + T^{-1}), \quad Q/\Omega_c = \frac{1}{2}(T - T^{-1}). \quad (2.19a,b)$$

Since $Q/\Omega_c > 0$, (2.19b) implies that (a) $1 < T < \infty$, $\Omega/\Omega_c > 1$ or (b) $-1 < T < 0$, $\Omega/\Omega_c < -1$. Note that the limiting case $Q=0$ ($\Omega = \pm \Omega_c$) corresponds to $T=1$ or $T=-1$, which is the same as in (2.16). For $Q \neq 0$, (2.18) leads to

$$q = m\pi + (\alpha - \beta + \gamma_1 - \gamma_2), \quad (2.20)$$

where m is an integer and

$$\tan \gamma_1 = \frac{\sin 2\alpha}{T - \cos 2\alpha}, \quad \tan \gamma_2 = \frac{\sin 2\beta}{T - \cos 2\beta}. \quad (2.21a,b)$$

Here γ_1 and γ_2 lie in $(-\pi/2, \pi/2]$. The eigenfunctions are

$$\hat{A}(x) = a (e^{-iq(x_0-x)/L} + T^{-1} e^{i2(\alpha + \gamma_1)} e^{iq(x_0-x)/L}), \quad (2.22a)$$

$$\hat{B}(x) = a (T^{-1} e^{-iq(x_0-x)/L} + e^{i2(\alpha + \gamma_1)} e^{iq(x_0-x)/L}). \quad (2.22b)$$

The algorithm for finding the eigenvalues is similar to that in § 2.1. For given α and β , we select a sequence of values of T from an appropriate range. For each T , we determine γ_1 and γ_2 using (2.21), and q from (2.20) for some integer m . From (2.19), Ω and Ω_c are obtained for given water depth and tank length, and ϵ follows from (2.6). Note that $m \ll N$ for the asymptotic theory to be accurate, and it should also be selected so that $q > 0$.

The multiple values of q are necessary, allowing us to see how the normal modes, in the neighbourhood of the Bragg frequency, connect to those of the flat-bottomed tank as $\epsilon \rightarrow 0$: the mode associated with $1 \leq m \ll N$ connects to the $(N+m)$ th mode of the flat-bottomed tank for $\Omega > 0$, and to the $(N-m)$ th mode for $\Omega < 0$; the mode associated with $m=0$ connects to the N th mode provided that $\alpha > \beta$ if $\Omega > 0$ or $\alpha < \beta$ if $\Omega < 0$. Only one or two of these will enter the wedge of exponential behaviour as ϵ becomes positive, but the others are still present. Detailed explanation is given in Appendix A.1.

3. Exact solutions using continued fractions

The asymptotic theory just described is superior in illuminating the physics. Still, it is approximate, and only applicable when the corrugations are of small amplitude and the tank is long. Moreover, it is only appropriate for normal modes with frequencies near ω_B . These limitations can be largely overcome, though at the expense of somewhat more complicated calculations, and perhaps a less transparent physical picture.

In the following we consider only the linear theory of waves with simple harmonic time dependence. We do *not* assume that the bottom corrugations are of infinitesimal amplitude, though for simplicity we shall take them to be of a specific form, approximately sinusoidal. We shall in this section construct the solutions for an infinitely long tank (or channel), and return in §5 to the normal mode problem for a tank with vertical endwalls. From the linear wave theory, the velocity potential $\phi(x, z, t)$ should satisfy

$$\nabla^2 \phi = 0 \quad \text{for } -h + h_b \leq z \leq 0, \quad -\infty < x < \infty, \quad (3.1)$$

$$\phi_z = \phi_x h_{b,x} \quad \text{at } z = -h + h_b, \quad (3.2)$$

$$\phi_{tt} + g\phi_z = 0 \quad \text{at } z = 0, \quad (3.3)$$

where h_b is the profile of the bottom corrugations. For mathematical convenience, we shall use a conformal map, i.e.

$$k_B x = \xi - \epsilon b \sin 2\xi \cosh 2\eta, \quad k_B z = \eta - \epsilon b \cos 2\xi \sinh 2\eta, \quad (3.4a,b)$$

where

$$b = k_B h / \sinh(2k_B h). \quad (3.5)$$

Furthermore, we assume that the corrugations have the form

$$h_b = \epsilon h \cos 2\xi, \quad \text{where } \xi - \epsilon k_B h \coth(2k_B h) \sin 2\xi = k_B x, \quad (3.6)$$

so that the undisturbed free surface $z=0$ is mapped onto $\eta=0$ and the bottom $z=-h+h_b$ onto $\eta=-k_B h$, making the actual flow domain a strip on the mapped plane. For small ϵ , it is clear that $h_b \simeq \epsilon h \cos(2k_B x)$. The transformation (3.4) has been used for a somewhat similar purpose by Benjamin, Boczar-Karakiewicz & Pritchard (1987). We shall restrict attention to $\epsilon \leq \epsilon_*$, where

$$\epsilon_* = \tanh 2k_B h / (2k_B h), \quad (3.7)$$

for when $\epsilon > \epsilon_*$, x ceases to be a monotonic function of ξ and solutions calculated in the (ξ, η) plane do not seem to have any meaning in the (x, z) plane. As $\epsilon \rightarrow \epsilon_*$ from below, the crests of the bottom corrugations become cusps, with infinite slope. Since $\epsilon_* < 1$, these crests do not penetrate the surface. Some bottom profiles are shown in figure 5 for $\epsilon \leq \epsilon_*$ and $k_B h = 0.5$.

For periodic motion of angular frequency ω we may set $\phi = e^{-i\omega t} \varphi(x, z) + \text{c.c.}$ From (3.1)–(3.3), we write the equations for determining φ , in the (ξ, η) plane, as follows.

$$\varphi_{\xi\xi} + \varphi_{\eta\eta} = 0 \quad \text{for } -k_B h \leq \eta \leq 0, \quad -\infty < \xi < \infty, \quad (3.8)$$

$$\varphi_\eta = 0 \quad \text{at } \eta = -k_B h, \quad (3.9)$$

$$\varphi_\eta = \omega^2 (gk_B)^{-1} (1 - 2\epsilon b \cos 2\xi) \varphi \quad \text{at } \eta = 0. \quad (3.10)$$

We shall use

$$\lambda = \omega^2 (gk_B)^{-1} \quad (3.11)$$

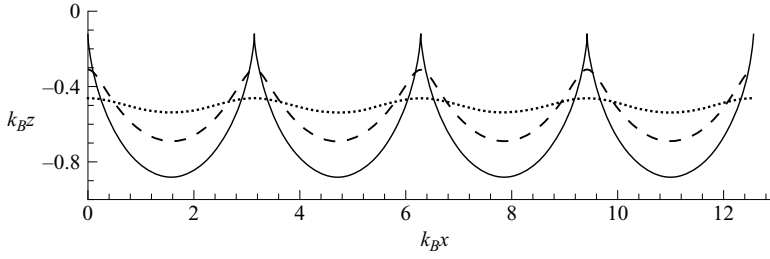


FIGURE 5. Profiles of bottom corrugations. $k_B h = 0.5$. $\cdots\cdots$, $\epsilon = 0.1\epsilon_*$; $---$, $\epsilon = 0.5\epsilon_*$; $---$, $\epsilon = 1.0\epsilon_*$.

as a dimensionless measure of angular frequency. For perfect tuning to Bragg resonance frequency, i.e. $\omega = \omega_B$, $\lambda_B = \tanh k_B h$.

Following the general ideas of Floquet theory, we shall seek solutions of this problem as superpositions of ‘Floquet solutions’, which have the form of a periodic function of ξ , multiplied by an exponential in ξ . We are particularly interested in the extension to finite ϵ of those exponentially decaying (or growing) solutions close to the Bragg resonance frequency which we have discussed in §2 using the asymptotic theory (however, for small ϵ). A solution of this kind cannot have any net energy flux, since it goes to zero at large distance in one direction or the other. Thus if we follow a family of such solutions as $\epsilon \rightarrow 0$, the limiting flat bottom solution should also have zero energy flux, and hence it cannot in fact be either of the propagating waves alone, but must be a standing wave combination of both (of which there are also two independent ones, e.g. $\cos k_B x$ and $\sin k_B x$). In order to have such a family of solutions as $\epsilon \rightarrow 0$, we need to stay inside the wedge of exponential behaviour: see figure 4. In particular, if we let $\epsilon \rightarrow 0$ at a fixed frequency, we must set $\omega = \omega_B$, i.e. the ‘perfectly tuned’ family. Other families could be chosen, of course, so long as $\omega(\epsilon)$ remains inside the wedge (hence $\omega \rightarrow \omega_B$ as $\epsilon \rightarrow 0$). This remark will be relevant to the form of representation most suitable for the Floquet solutions, to which we now turn.

3.1. ‘Propagating’ waves

It is readily seen that the Laplace equation (3.8) and the bottom boundary condition (3.9) can be satisfied by a velocity potential of the Floquet form

$$\varphi = e^{\mu\xi} \sum_{n=-\infty}^{\infty} D_n e^{in\xi} \frac{\cosh [(n - i\mu)(\eta + k_B h)]}{\cosh [(n - i\mu)k_B h]}, \tag{3.12}$$

where μ is the Floquet exponent (complex in general) and D_n the Fourier coefficients of the periodic factor of φ , independent of η . From the surface boundary condition (3.10), we find a recurrence relationship among the Fourier coefficients, i.e.

$$L_n D_n = D_{n-2} + D_{n+2}, \tag{3.13}$$

where

$$L_n := -(\epsilon b \lambda)^{-1} \{(n - i\mu) \tanh [(n - i\mu)k_B h] - \lambda\}. \tag{3.14}$$

Note that the cases of even and odd n are not coupled, and may be considered separately. In fact, a solution represented with only odd n in (3.12) can be transformed, by replacing μ with $\mu + i$ or $\mu - i$, into a solution represented with only even n . Even if we stick to a representation with only odd n , by replacing μ with $\mu \pm 2i$ we should

get different representations of the same sort. This artificial non-uniqueness may be suppressed by requiring, say, that $-1 < \text{Im } \mu \leq 1$.

A solution of the form (3.12) would resemble that described by the asymptotic theory if μ is small of $O(\epsilon)$, and ω is close to ω_B . In such cases, the dominant Fourier coefficients are $D_{\pm 1}$, and the representation with odd n would be more convenient. Furthermore, $L_{\pm 1}$ can be moderate even with ϵ small, while other L_n are then necessarily large in comparison. We shall thus first take this case of odd n s, though later we shall also find the representation with even n to be useful for other solutions (see §3.2). We can write (3.13) in two different forms:

$$D_n/D_{n-2} = 1/(L_n - D_{n+2}/D_n), \quad D_n/D_{n+2} = 1/(L_n - D_{n-2}/D_n). \quad (3.15a, b)$$

L_n depends on λ , ϵ , $k_B h$ and μ . We think of λ , ϵ and $k_B h$ as being given, and try to find μ so that the Fourier series for φ is convergent. Thus we shall write $L_n(\mu)$, suppressing the dependence on the other parameters. Using (3.15a) repeatedly, we obtain

$$D_1/D_{-1} = CF_1(\mu), \quad (3.16)$$

where the continued fraction $CF_1(\mu)$ follows the definition

$$CF_n(\mu) = \frac{1}{L_n(\mu) - \frac{1}{L_{n+2}(\mu) - \frac{1}{L_{n+4}(\mu) - \dots}}}. \quad (3.17)$$

A glance at (3.14) shows that $L_{-n}(\mu) = L_n(-\mu)$. Thus, $CF_{-n}(\mu) = CF_n(-\mu)$. As noted above, for small ϵ we may expect to find L_1 moderate for suitable small μ and ω near ω_B , but in any case the L_n always become increasingly large as n increases. Thus we may expect CF_1 to converge fairly rapidly. This is consistent with $D_n/D_{n-2} \rightarrow 0$ as $n \rightarrow +\infty$, as we wish for convergence of the Fourier series. From (3.15b), we have similarly $D_{-1}/D_1 = CF_1(-\mu)$, whose convergence is consistent with that of the Fourier series for $n \rightarrow -\infty$. For this to be consistent with (3.16), we must require

$$CF_1(\mu)CF_1(-\mu) = 1. \quad (3.18)$$

The possible Floquet exponents μ are determined by this basic equation, given λ , ϵ and $k_B h$. Evidently, if μ is real then $CF_1(-\mu) = CF_1(\mu)^*$, the complex conjugate, and so $|CF_1(\mu)| = 1$. These continued fractions do indeed converge rapidly, and both the computation of $CF_1(\mu)$ and the numerical solution of (3.18) are quite easy. We shall give a number of results of such computations in §4. A few remarks are noted.

First, suppose we fix a value of ω distinct from ω_B , and let ϵ get small. If we are considering a Floquet-type solution, and its exponent has a real part which is zero or small, then our solution must be approaching some combination of the two propagating waves corresponding to that frequency for the flat bottom; their wavenumbers $\pm k$ satisfy $\omega^2 = gk \tanh kh$. In this case for small enough ϵ we are certainly outside the wedge, and the asymptotic theory indicates that we have a periodically modulated wave (oscillatory behaviour), rather than an exponentially varying one. The argument given above for approaching a standing wave as $\epsilon \rightarrow 0$ is no longer applicable outside the wedge. Indeed the modulated wave might well carry a net energy flux one way or the other. In this case the Floquet-type solution does approach a propagating wave.

Second, if we allow ω to be sufficiently different from ω_B (so is λ from λ_B), the Floquet-type solution includes higher-order Bragg resonance, in which the water

waves have a wavenumber equal not to half that of the bottom corrugations, but to two or three halves times it, i.e. $k = m(k_B/2)$ with m being integers. This feature is not suggested by the asymptotic theory (at least not without a significant modification), as the asymptotic theory requires ω be sufficiently close to ω_B . While we shall not go into this any further here, it appears likely that the asymptotic theory could be modified to investigate slowly varying combinations of left- and right-going propagating waves of these wavenumbers (as well as of other integral multiples of k_B).

Finally, as a historical note, it is interesting to observe that while the use of continued fractions in more or less the way we have done here is familiar in connection with the study of Mathieu functions, it can be traced back much earlier, indeed in hydrodynamics. In the 1770s Laplace began his researches on tides on a rotating globe and in that context made use of a method essentially equivalent to one using continued fractions, which he explicitly brought in while presenting these results in the *Mécanique Céleste* of 1799. Such techniques were also extensively used in the further development of tidal theory by Kelvin, Darwin, and Hough in the last quarter of the nineteenth century; see Lamb's *Hydrodynamics*, sixth edition, Chapter VIII.

3.2. Evanescent waves

The evanescent waves for a flat bottom ($\epsilon = 0$) are obtained with a velocity potential of the form

$$\varphi = e^{\mu\xi} \cos[\mu(\eta + k_B h)] = e^{\mu\xi} \cosh[-i\mu(\eta + k_B h)] \tag{3.19}$$

with the 'dispersion relation' $\lambda = -\mu \tan(\mu k_B h) = -i\mu \tanh(-i\mu k_B h)$, where λ is the same as in (3.11). (3.19) is just like the $n = 0$ term in (3.12), and the dispersion relation is obtained by setting $L_n = 0$ in the case $n = 0$ of (3.14). Thus it is convenient in finding the extension to $\epsilon > 0$ of the evanescent waves to use the even n case in the representation (3.12). We can thus expect that the principal term in the series, when ϵ is small, will be that for $n = 0$ and the Floquet exponent will be close to one of the solutions of $\lambda = -\mu \tan(\mu k_B h)$. We call the positive solutions of this equation μ_1^0, μ_2^0, \dots , and evidently $k_B h \mu_n^0$ lies in the interval $(n\pi - 1/2\pi, n\pi)$, getting close to $n\pi$ as n increases; $-\mu_n^0$ are the negative solutions.

The recurrence relationship (3.13) and the definition of $L_n(\mu)$ in (3.14) are the same, regardless of n being odd or even. We thus write from (3.13) the following two forms:

$$D_0/D_2 = 1/CF_2(\mu), \quad D_2/D_0 = L_0(\mu) - CF_2(-\mu), \tag{3.20a,b}$$

where CF_2 follows (3.17). The consistency of these two expressions means

$$L_0(\mu) = CF_2(\mu) + CF_2(-\mu). \tag{3.21}$$

This equation is the analogue for evanescent waves of (3.18) for 'propagating waves'. As in the latter case, if μ is a solution, so is $-\mu$. Note that if μ is real, $CF_2(\mu)$ and $CF_2(-\mu)$ are complex conjugates; if μ is pure imaginary, the CF_2 s are both real.

3.3. Wave forms

After the Floquet exponent μ has been obtained for the 'propagating' and evanescent waves, we still have to find the Fourier coefficients D_n which give the periodic factor in (the extension to $\epsilon > 0$ of) each case. In the propagating case, when μ is real (i.e. inside the wedge of exponential behaviour), the CF_1 s are of modulus 1: cf. § 3.1. Suppose $CF_1(\mu) = e^{i\theta}$. If we normalize so that $D_1 = e^{i\theta/2}$, we see from (3.16) that $D_{-1} = e^{-i\theta/2}$. It is then easy to show inductively from (3.13) that D_n and D_{-n} are conjugates for all odd n . Thus, with this normalization the sum of the Fourier series is real. Since L_n increases rapidly with n , D_{n+2} for large n would be given by (3.13) as the

difference of two large and nearly equal numbers. A stable way to calculate D_n is as follows.† From (3.15a), $D_n/D_{n-2} = CF_n(\mu)$. We set $R_j := D_{2j+1}/D_{2j-1}$, and select some largish integer J with the intention of computing $D_1, D_3, \dots, D_{2J+1}$. We first compute $R_J = CF_{2J+1}$ directly from (3.17), then successively calculate $R_{j-1} = (L_{2j-1} - R_j)^{-1}$, for $j = J, J-1, \dots, 2$. Starting with D_1 , normalized as above, we then compute, $D_{2j+1} = R_j D_{2j-1}$ for $j = 1, 2, \dots, J$. The calculation of $CF_n(\mu)$ using (3.17) is done by the usual method: see Appendix A.2. The Floquet solution for the other root $-\mu$ of (3.18) can be obtained from the $+\mu$ solution. This is done simply by reversing the sign of μ in (3.12) and using for the Fourier coefficients the complex conjugates of those found for $+\mu$.

Essentially the same method applies, with even n , for the evanescent waves. In this case the μ_j s are also found to be real and it is convenient to normalize by choosing $D_0 = 1$. It is then readily verified that D_{2j} and D_{-2j} are complex conjugates, so again the sum of the Fourier series is real. Also the Fourier coefficients for the solutions corresponding to the negative μ_j s are the conjugates of those for the positive ones.

4. Results

4.1. Range of exponential behaviour

In the asymptotic theory, the exponential behaviour occurs when $|\omega - \omega_B| = |\Omega| < \Omega_c$. In the exact theory it occurs when $\text{Re } \mu \neq 0$. We have indeed found that (3.18) has pure real solutions for μ , if λ is sufficiently close to λ_B for $0 < \epsilon \leq \epsilon_*$. As λ moves away from λ_B on either side, μ eventually goes to zero and then becomes pure imaginary, corresponding to the sinusoidally modulated waves (i.e. oscillatory behaviour). The boundaries of the exponential region, where $\mu = 0$, are the cutoff values λ_{c^\pm} , where $\lambda_{c^-} < \lambda_B < \lambda_{c^+}$. The cutoff frequencies are $\omega_{c^\pm}^2 = gk_B \lambda_{c^\pm}$, which are the analogues of $\omega_B \pm \Omega_c$ in the asymptotic theory. The values λ_{c^\pm} are obtained by finding roots of $|CF_1(0)| = 1$, given $k_B h$ and ϵ .

For the asymptotic theory, $(\omega_{c^\pm}/\omega_B)_{asy} = 1 \pm (\epsilon/\epsilon_*) (4 \cosh 2k_B h)^{-1}$, and for the exact theory, $(\omega_{c^\pm}/\omega_B)_{ex} = (\lambda_{c^\pm}/\lambda_B)^{1/2}$. In figure 6, ω_{c^\pm}/ω_B are plotted against ϵ/ϵ_* , for $k_B h = 0.1, 0.5$, and 1.0 (from (3.7), $\epsilon_* = 0.9869, 0.7616, 0.4820$ correspondingly). For small ϵ/ϵ_* , the asymptotic results agree very well with the exact values at all water depths. This is expected. At large $k_B h$, the excellent agreement holds even up to $\epsilon = \epsilon_*$, which seems well beyond what might be expected. The asymptotic theory deviates noticeably from the exact theory at relatively shallower water depth, e.g. $k_B h \leq 0.5$, and for large amplitudes of corrugations. In particular, ω_{c^\pm} are not symmetrical about ω_B according to the exact theory, and no longer linear in ϵ/ϵ_* either. However, the widths of the wedge, $(\omega_{c^+} - \omega_{c^-})/\omega_B$ at all values of ϵ/ϵ_* , are still accurately represented by the asymptotics.

4.2. Floquet exponents

Inside the wedge of exponential behaviour, the Floquet exponent μ is real, while outside it (at least for some distance), μ is pure imaginary. Thus, a graph of μ^2 as

† This method may well have been used by Laplace. It was certainly used by Nathaniel Bowditch (1773–1838), the early American astronomer and navigator who translated the *Mécanique Céleste* (volumes I–IV) into English, giving very extensive annotation (more than doubling Laplace's text). Bowditch's translation was not published (1832, Vol. II) until after the death of Laplace, but was done much earlier and had been praised by Laplace: 'I am sure that M. Bowditch comprehends my work, for he has not only detected my errors, but he has also shown me how I came to fall into them' (Struik 1991, p. 231).

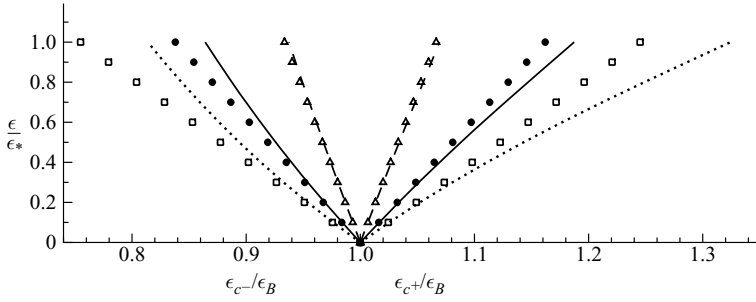


FIGURE 6. Graphs of ω_{c-}/ω_B (< 1) and ω_{c+}/ω_B (> 1) as functions of ϵ/ϵ_* for different water depths. Exact theory: $\cdots\cdots$, $k_B h = 0.1$; —, $k_B h = 0.5$; ---, $k_B h = 1.0$. Asymptotic theory: \square , $k_B h = 0.1$; \bullet , $k_B h = 0.5$; \triangle , $k_B h = 1.0$.

a function of λ is convenient for display both inside ($\mu^2 > 0$) and outside ($\mu^2 < 0$) the exponential regime. A clarification remark is necessary. For the exact solution, the Floquet exponent μ is for ξ , which is normalized using k_B . The analogue of a Floquet solution of the asymptotic theory is a solution of (2.5) in which A and B are proportional to $e^{-i\Omega t \pm qx/L}$, where q is related to Ω by (2.9). In terms of $k_B x$, the Floquet exponent of the asymptotics should then be $\mu_{asy} = \pm q/(k_B L)$. From (2.9) and (2.6), and noting that $\omega - \omega_B = \Omega$, we get, after some algebra,

$$\mu_{asy}^2 = (b + \frac{1}{2})^{-2} \{ \frac{1}{4} b^2 \epsilon^2 - [(\lambda/\lambda_B)^{1/2} - 1]^2 \}, \tag{4.1}$$

where b is given in (3.5). It is worth pointing out that μ for the exact theory, though introduced for ξ , is in fact also the Floquet exponent for $k_B x$. This is seen as follows. Using the conformal mapping (3.4), one can show that $e^{\mu\xi} P(\xi, \eta) = e^{\mu k_B x} P_1(k_B x, k_B z)$, where

$$P_1(k_B x, k_B z) = e^{-\mu \epsilon b \sin 2\xi \cosh 2\eta} P(\xi, \eta). \tag{4.2}$$

Clearly, if $P(\xi, \eta)$ is periodic in ξ with period π or 2π , so is $P_1(k_B x, k_B z)$ in $k_B x$ with same period. In other words, when $P(\xi, \eta)$ is the periodic factor in terms of ξ , $P_1(k_B x, k_B z)$ is the periodic factor in terms of $k_B x$, corresponding to the same Floquet exponent μ .

Figure 7(a) shows μ^2 as a function of λ at $k_B h = 0.2$ and for different values of ϵ , comparing the exact theory and the asymptotics. As is anticipated, the discrepancy becomes greater as the amplitude and steepness of the corrugations increase. This is partially because the asymptotic method is based on small ϵ , but may in part be due to the fact that it also uses a purely sinusoidal bottom profile, while the profile used for the exact theory (in the $x-z$ plane) is less sinusoidal as ϵ increases.† In figure 7(b), similar data are plotted for $\epsilon = 0.6$, and for $k_B h = 0.2, 0.6, 1.0$ and 1.2 , showing the effects of water depth. The asymptotic theory is generally accurate, except in sufficiently shallow water depth.

† To investigate this, however, we should either have to give up the advantages of the conformal map into a strip and somehow work in the (x, z) plane, or find such a map for the region with a truly sinusoidal bottom into a strip, in which case we should have a modified (3.10) with many harmonics. In either case it seems that we should have to deal with more general infinite determinants than the tri-diagonal kind which are equivalent to continued fractions.

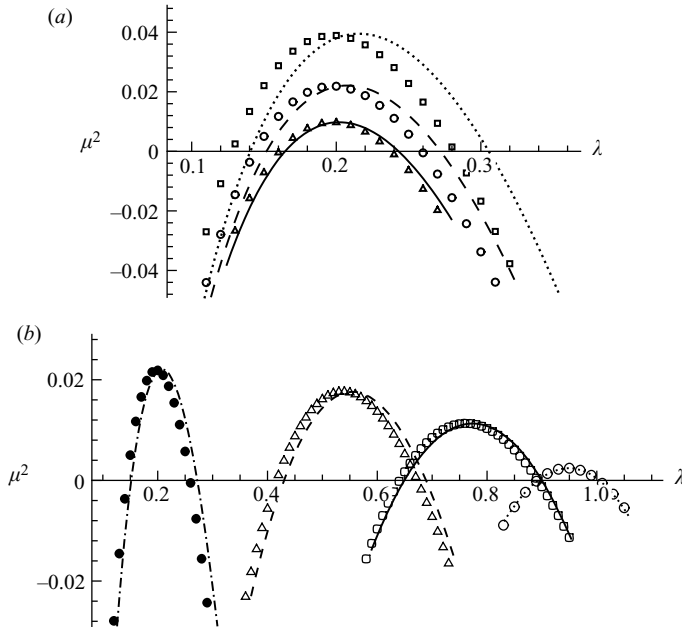


FIGURE 7. (a) Graphs of μ^2 as a function of λ for $k_B h = 0.2$. Exact theory: —, $\epsilon = 0.4$; ---, $\epsilon = 0.6$; ·····, $\epsilon = 0.8$. Asymptotic theory: Δ , $\epsilon = 0.2$; \circ , $\epsilon = 0.4$; \square , $\epsilon = 0.8$. (b) Graphs of μ^2 as a function of λ for $\epsilon = 0.6$. Exact theory: -·-·-, $k_B h = 0.2$; ---, $k_B h = 0.6$; —, $k_B h = 1.0$. ·····, $k_B h = 1.8$; Asymptotic theory: \bullet , $k_B h = 0.2$; Δ , $k_B h = 0.6$; \square , $k_B h = 1.0$; \circ , $k_B h = 1.8$.

4.3. Periodic factor for ‘propagating’ waves

The procedure for calculating the Fourier coefficients has been discussed in §3.3. In this way we have calculated D_1, D_3, \dots, D_{11} , for $k_B h = 0.1, \dots, 2.0$, and for each of these for ranges of λ and ϵ covering the exponential regime. However, it is found that D_n for $n > 5$ are insignificant ($|D_5/D_1|_{\max} < 0.0023$ and mostly considerably smaller; $|D_{11}/D_1| \sim 10^{-8}$ to 10^{-11}). The periodic factor $P(\xi, \eta)$, i.e. the Fourier series in (3.12), can thus be computed with sufficient accuracy by using just D_1, D_3, D_5 and their conjugates. This could be done for any η , but it is of greatest interest at the free surface $\eta = 0$. The free surface periodic factor in terms of $k_B x$ is $P_1(k_B x, 0)$, and can be calculated parametrically from (4.2) with $\eta = 0$. We give some sample graphs of $P_1(k_B x, 0)$ and $P(\xi, 0)$. In figure 8, $k_B h = 0.3$, $\epsilon/\epsilon_* = 0.5$ and the values of λ (in increasing order) run across the exponential regime from its left boundary to the right. In figure 9, we choose $\epsilon/\epsilon_* = 1.0$ and vary $k_B h$. The value of λ is in the middle of the exponential regime for the given $k_B h$ and ϵ . Finally, in figure 10 we illustrate the effect of increasing ϵ (from $0.1\epsilon_*$ to ϵ_*), for $k_B h = 0.3$ and λ being in the middle of the exponential regime. Deviations from the purely sinusoidal wave form of the asymptotic theory are most pronounced when $k_B h$ is smaller (i.e. the depth is small compared to the Bragg resonant wavelength), and when ϵ is closer to ϵ_* (i.e. the peaks of the bottom corrugations are sharper, and nearer the surface). These deviations are more pronounced when $k_B x$ is the independent variable than they are in terms of ξ . The coordinate transformation seems to bring in higher harmonics to a greater extent than do D_3, D_5, \dots, D_n .

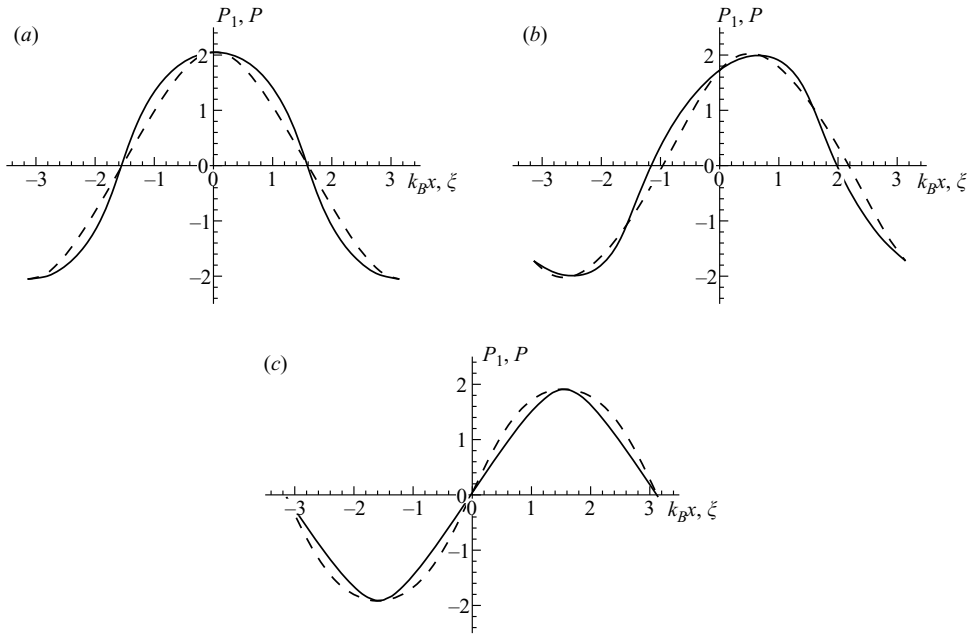


FIGURE 8. Periodic factors at $k_Bh = 0.3$, $\epsilon/\epsilon_* = 0.5$ and for different values of λ . —, $P_1(k_Bx, 0)$ versus k_Bx ; ---, $P(\xi, 0)$ versus ξ . (a) $\lambda = 0.23953$, (b) $\lambda = 0.26539$, (c) $\lambda = 0.36488$.

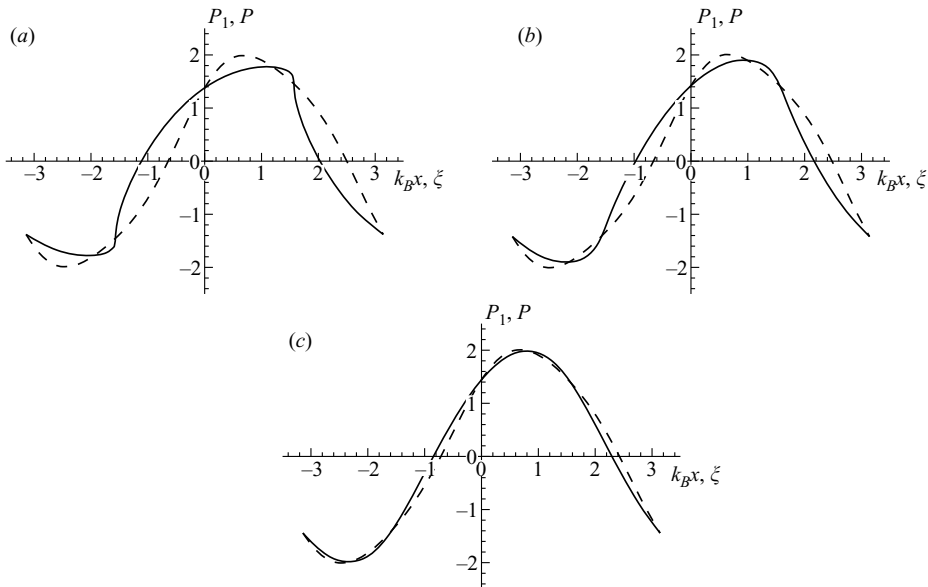


FIGURE 9. Periodic factors at $\epsilon/\epsilon_* = 1.0$, and for different values of k_Bh . The value of λ is in the middle of the exponential regime for given ϵ and k_Bh . —, $P_1(k_Bx, 0)$ versus k_Bx ; ---, $P(\xi, 0)$ versus ξ . (a) $k_Bh = 0.1$, (b) $k_Bh = 0.5$, (c) $k_Bh = 1.0$.

5. Normal modes in a tank

We now wish to use these results to discuss the normal mode problem for a tank with vertical endwalls, which we have considered in §2 using the asymptotic theory.

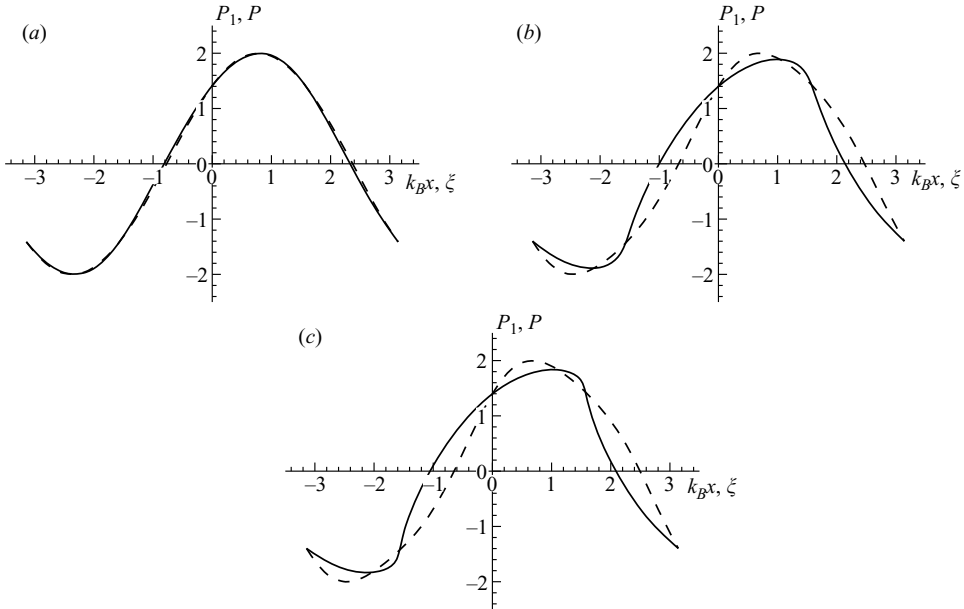


FIGURE 10. Periodic factors at $k_B h = 0.3$, $\lambda = 0.29131$, and for different values of ϵ . —, $P_1(k_B x, 0)$ versus $k_B x$; - - -, $P(\xi, 0)$ versus ξ . (a) $\epsilon = 0.1\epsilon_*$, (b) $\epsilon = 0.8\epsilon_*$, (c) $\epsilon = 1.0\epsilon_*$.

There are some complications to this, which make the problem quite different from the flat bottom case ($\epsilon = 0$). First, the ends are in general not at constant values of ξ (or if they were taken to be at constant ξ they would not be at constant x). In the (ξ, η) plane, let $\xi = \xi_0(\eta)$ and $\xi = N\pi + \xi_1(\eta)$ be the images of $x = x_0$ and $x = x_0 + L$, respectively. From (3.4a), we have

$$\alpha = \xi_0 - \epsilon b \sin 2\xi_0 \cosh 2\eta, \quad \beta = \xi_1 - \epsilon b \sin 2\xi_1 \cosh 2\eta, \quad (5.1a, b)$$

where α, β and N are the same as in (2.7). If we identify $2\xi_0$ (or $2\xi_1$) with E , 2α (or 2β) with M , and $2\epsilon b \cosh 2\eta$ with e , both equations in (5.1) take the form of

$$M = E - e \sin E, \quad (5.2)$$

which is known as Kepler's equation, arising in the theory of the elliptic orbits of the planets (E is the 'eccentric anomaly', e orbital eccentricity and M the 'mean anomaly' which is proportional to the time since the planet was at perihelion). In our application, the effective eccentricity e has a maximum value ϵ/ϵ_* occurring at $\eta = -k_B h$, given b in (3.5). Since we have restricted to $\epsilon/\epsilon_* \leq 1$, the cases of interest here correspond exactly to elliptic orbits in the context of celestial mechanics. Kepler in 1627 published tables to facilitate the solutions to (5.2). Since then many algorithms have been developed. An interesting historical account is in Colwell (1993). We have used the first approximation in Markley (1996). Details of the algorithm are given in Appendix A.3.

As an example we may take the illustration used in §2.1, in which $\alpha = 5\pi/12$, $\beta = 4\pi/15$ and $N = 16$. Also, $k_B h = 0.5$ and $\epsilon = 0.1048$ which makes $\epsilon/\epsilon_* = 0.1376$, hence $e = 0.0892 \cosh 2\eta$. For the left end, $M = 5\pi/6$, the calculation shows that $\xi_0(0) = 1.330$ at the surface and $\xi_0(-k_B h) = 1.340$ at the bottom. Similarly, $\xi_1(0) = 0.881$ and $\xi_1(-k_B h) = 0.904$. Since the length of the domain is about 16π , it would be rather difficult to distinguish this region from a rectangle in any ordinary diagram. The

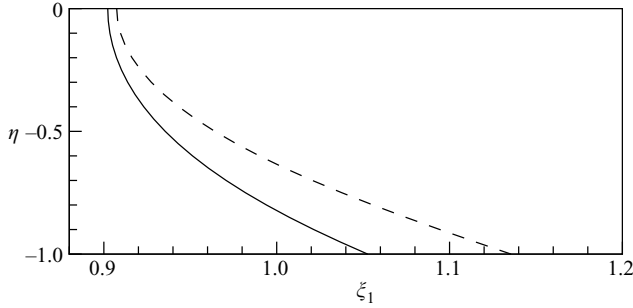


FIGURE 11. The shape of the right endwall $\xi_1(\eta)$ in the (ξ, η) plane: —, $\beta = 4\pi/15$, $k_B h = 1.0$ and $\epsilon/\epsilon_* = 0.5$; ---, $\beta = 32\pi/127$ (close to $4\pi/15$), $k_B h = 1.0$ and $\epsilon/\epsilon_* = 0.9$. Note that the actual position of the right endwall is $\xi = N\pi + \xi_1$.

deviation from the vertical is somewhat more pronounced, if ϵ/ϵ_* is nearer 1 and α or β is near $\pi/4$ (or $-\pi/4$). It is also more noticeable if $k_B h$ is larger, for then $\cosh 2\eta$ varies more over the range from the surface to the bottom. All of these just mentioned bring about a more marked variation in the effective eccentricity, and it is this variation in eccentricity that causes the variation of ξ_0 or ξ_1 with η . The shape of the right end $\xi_1(\eta)$ is shown in figure 11 for the case $\beta = 4\pi/15$, $k_B h = 1.0$, and $\epsilon/\epsilon_* = 0.5$. Also included is $\xi_1(\eta)$, for $\beta = 32\pi/127$ (close to $4\pi/15$), $k_B h = 1.0$ and $\epsilon/\epsilon_* = 0.9$, which would just be the reflection of $\xi_0(\eta)$ if we took $\alpha = -\beta$. However, even in this extreme case the difference in the total length of the tank is less than 0.5, which is only about 1% of either total length (approximately $N\pi$) when $N = 16$. Note that N cannot be taken too small without losing much of the Bragg resonance effect.

In the flat bottom case, the propagating waves and all the evanescent waves are found by separation of variables, and the z dependences are the eigenfunctions of a Sturm–Liouville problem, hence orthogonal. This orthogonal structure is useful to solve boundary value problems with data on vertical boundaries (e.g. the linearized wavemaker problem). It can also be helpful when the endwalls are not quite vertical (and simple standing waves do not suffice) by linearizing the boundary conditions. In the present case, however, even though the endwalls are not far from vertical in the (ξ, η) plane, this linearization of the boundary conditions has less appeal. This is because the ‘propagating’ and evanescent waves no longer have any sort of orthogonal structure along a vertical boundary ($\xi = \text{constant}$). They do not have any orthogonality along the actual boundaries $\xi = \xi_0$ and $\xi = N\pi + \xi_1$ either, but if we are going to use some other way (such as a collocation method) of applying the endwall boundary conditions, we might as well use the actual endwall positions.

Since the mapping is conformal, the boundary conditions remain that the normal derivative of φ should be zero at the endwalls, i.e.

$$\varphi_\xi - \xi_{0,\eta}\varphi_\eta = 0 \quad \text{at} \quad \xi = \xi_0(\eta), \tag{5.3a}$$

$$\varphi_\xi - \xi_{1,\eta}\varphi_\eta = 0 \quad \text{at} \quad \xi = N\pi + \xi_1(\eta). \tag{5.3b}$$

By differentiating (5.1) with respect to η , we obtain $\xi_{0,\eta}$ and $\xi_{1,\eta}$. Thus once $\xi_0(\eta)$ and $\xi_1(\eta)$ are solved from (5.1); evaluation of (5.3) is straightforward. Note that ξ_0 , ξ_1 , $\xi_{0,\eta}$ and $\xi_{1,\eta}$ are obtained as functions of η , given the geometric parameters $k_B h$, ϵ (or ϵ/ϵ_* , ϵ_* being a function of $k_B h$), α , β and N describing the flow domain in the (ξ, η) plane. $k_B h$ and ϵ characterize the geometry of the corrugation wave; the others

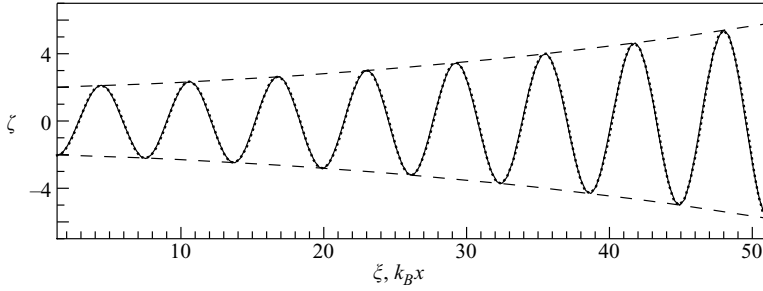


FIGURE 12. The profile of the surface elevation (at $t=0$) from exact solutions: —, as a function of ξ ; $\cdots\cdots$, as a function of $k_B x$. The envelope of the surface profile (dashed curves) is calculated using the asymptotic theory and is shown for comparison. Parameters are $k_B h = 0.5$, $\epsilon/\epsilon_* = 0.1376$, $\alpha = 5\pi/12$, $\beta = 4\pi/15$, $N = 16$.

define the location of the endwalls. With the adjunction of a dimensional length, say the water depth h , the physical variables in the (x, z) plane are recovered.

Given $k_B h$, ϵ and λ , the L_n and thus the CF_n are determined as functions of μ . In the ‘propagating’ case, $+\mu$ and $-\mu$ can be determined from (3.18): cf. § 3.1. In the evanescent case, a sequence μ_1, μ_2, \dots and its negative $-\mu_1, -\mu_2, \dots$ are determined from (3.21): cf. § 3.2. For each of these we can find, as described in § 3.3, the corresponding functions φ , which we shall call φ^\pm for $\pm\mu$, and φ_j^\pm for $\pm\mu_j$. A general solution can then be constructed as

$$\varphi = C^- \varphi^- + C^+ \varphi^+ + \sum_{j=1, K} C_j^- \varphi_j^- + C_j^+ \varphi_j^+, \quad (5.4)$$

where the coefficients C are to be determined, and the truncation of the evanescent waves depends on the accuracy in satisfying the true boundary conditions. Since the main role of the evanescent waves is expected to be in adjusting the eigenfunctions near the ends of the region, it seems likely that those with negative Floquet exponents will be most important at the left end of the domain, and those with positive exponents at the right end. For this reason it is better in practice to modify slightly the normalization of φ_j^+ by replacing $e^{\mu_j \xi}$ by $e^{\mu_j (\xi - N\pi)}$, corresponding to shifting the origin of ξ from 0 to $N\pi$. This has no effect on the periodic factors for the evanescent waves (which have only even harmonics in their Fourier series), and has been done in (5.4).

Evaluating (5.3) at a set of $K+1$ values of η , we obtain a homogeneous linear system for the $2K+2$ coefficients C . The condition for λ to be an eigenvalue is that the matrix of the system is singular, given the geometric parameters. Once λ is found, a corresponding non-trivial solution of the system gives the coefficients C for (5.4) to provide the eigenfunction. This procedure, with the slight modifications needed when one is outside the wedge of exponential behaviour, is applicable to any of the eigenvalues, but we shall focus here on the eigenvalues close to λ_B where the Bragg resonance effects can have major consequences.

We have examined a number of cases, and describe some of the results here. First we take again the example cited in § 2.1, with $k_B h = 0.5$, $\alpha = 5\pi/12$, $\beta = 4\pi/15$, $N = 16$, and $\epsilon = 0.1048$ (i.e. $\epsilon/\epsilon_* = 0.1376$). From the exact solution, the ratio of the surface amplitudes at the two ends is 2.834, slightly (about 1.5%) less than 2.878 which is given by the asymptotic theory. $\lambda = 0.4615173$, which corresponds to $\omega/\omega_B = (\lambda/\lambda_B)^{1/2} = 0.9994$; so the frequency is not exactly ω_B , whereas it is in the asymptotic solution. The profile of the surface elevation (at $t=0$) is shown in figure 12. Also shown in this figure is the amplitude for the asymptotic theory, which

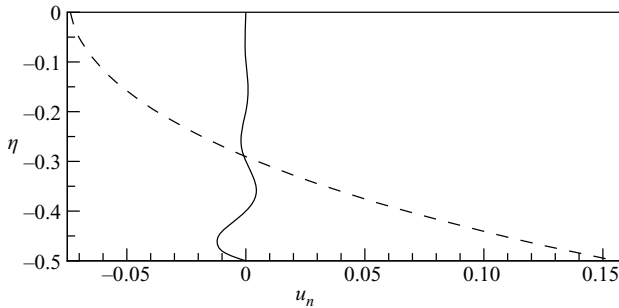


FIGURE 13. The normal velocity at the right endwall from exact calculation: —, using five of the evanescent waves and the two ‘propagating’ waves; ---, using only the two ‘propagating’ waves. Parameters are the same as in figure 12.

is calculated using (2.14), then transformed to the ξ coordinate and normalized so as to agree with the exact calculation at the right end. This asymptotic amplitude is then found to be about 1.5% less than the exact value at the left end, which is scarcely perceptible in the graph. These results indicate that, at least for this example, the asymptotic theory is satisfactory. We have also made the exact calculation and omitted the evanescent modes in reconstructing the surface elevation. This makes no difference throughout most of the domain, as is to be expected, but is of some minor significance near the ends (within two or three ξ units from either, and a difference less than 0.23%, in this example).

The evanescent components are, however, of great importance for the horizontal velocity near the ends. A combination of the two ‘propagating’ waves alone cannot satisfy, pointwise, the condition of zero normal velocity on the ends (except at $\epsilon = 0$). In our calculations we have in fact used only five of the evanescent modes (at each end) and together with the two ‘propagating’ waves have thus imposed the boundary conditions at the six collocation points $\eta = 0, -k_B h/5, -2k_B h/5, \dots, -k_B h$, at each of the two ends. In figure 13 we show (for the same example) the normal velocity at the right end for the computed eigenfunction, in comparison with the result when the evanescent modes are deliberately omitted. Evidently the solution including five of the evanescent modes comes much closer to satisfying the true boundary condition, though it only does so exactly at the collocation points.

In the asymptotic theory, (2.15) suggests that extreme values of the ratio of the surface amplitude at the two ends would occur with $\theta = \pi/2$ (i.e. $\omega = \omega_B$), $\alpha = \pi/2$, and β just slightly larger than $\pi/4$. In table 1 (see rows 1–4) we show examples of this ratio for the eigenfunction from the exact theory and the ratio of the frequency of the normal mode to ω_B , for several values of β approaching $\pi/4$ from above, taking $k_B h = 0.5$ and $N = 16$. The results from the asymptotic theory, following the procedure in § 2.1, are included for comparison. It is seen that both the amplitude and frequency ratios are quite close to the asymptotic results. Comparing the data in rows 4–7 of table 1, we see that the amplitude ratio decreases rapidly as the tank length is reduced while keeping other parameters the same. However, even when there are only about four corrugations in the tank, the ratio of the surface amplitude at the two ends can still be significantly greater than 1. Also notice that with the chosen parameters β , α and ϵ/ϵ_* the waves are no longer perfectly tuned according to the asymptotic theory for $N = 8, 6$ and 4. To obtain asymptotically perfect tuning for the smaller N , larger values of ϵ/ϵ_* are needed: see the last two rows in table 1.

N	β	ϵ/ϵ_*	Exact theory		Asymptotic theory	
			$\left \frac{\widehat{A}(x_0+L)}{\widehat{A}(x_0)} \right $	ω/ω_B	$\left \frac{\widehat{A}(x_0+L)}{\widehat{A}(x_0)} \right $	ω/ω_B
16	$4\pi/15$	0.1700	3.0345	0.9990	3.0930	1
16	$8\pi/31$	0.2120	4.3207	0.9984	4.4434	1
16	$16\pi/63$	0.2523	6.1050	0.9978	6.3333	1
16	$32\pi/127$	0.2935	8.5814	0.9970	8.9918	1
8	$32\pi/127$	0.2935	2.5798	1.0042	2.6234	1.0074
6	$32\pi/127$	0.2935	1.9723	1.0117	1.9836	1.0154
4	$32\pi/127$	0.2935	1.5387	1.0293	1.5299	1.0344
8	$32\pi/127$	0.5964	7.9892	0.9877	8.9918	1
6	$32\pi/127$	0.8038	7.4894	0.9777	8.9918	1

TABLE 1. The ratio of the eigenfunction (at the two endwalls) and the ratio of the frequency of the normal mode to ω_B , for $k_B h = 0.5$, $\alpha = \pi/2$, several values of β close to $\pi/4$, and for different tank lengths.

$k_B h$	1.0	1.0	1.5	1.5	1.5	2.0	2.0
ϵ/ϵ_*	0.5	0.7	0.5	0.7	0.9	0.7	0.9
ω/ω_B	0.9992	0.9970	1.0038	1.0021	1.0010	1.0054	1.0046
$\left \frac{\widehat{A}(x_0+L)}{\widehat{A}(x_0)} \right $	5.6621	12.6573	1.9739	2.7199	3.8188	1.4525	1.6367

TABLE 2. The ratio of the eigenfunction at the right and left end for various water depths, using exact theory. $\alpha = \pi/2$, $\beta = 32\pi/127$ and $N = 16$.

As we mentioned in §2.1, the value $k_B h = 0.5$ implies that the water level in the tank is very low, in the sense that the aspect ratio h/L is only about 0.01 for $N = 16$. It might be difficult to actually realize such a case in a laboratory tank. Increasing $k_B h$ makes the aspect ratio of the tank more reasonable, but requires larger ϵ to get a normal mode with frequency ω_B . In fact for $k_B h = 2.0$ we found, using the asymptotic theory, that for $\omega = \omega_B$ it requires $\epsilon = 0.3769$, which, in addition to being pretty large for a theory that assumes ϵ is infinitesimal, actually exceeds ϵ_* (0.2498 for $k_B h = 2.0$). However, there is no difficulty in computing examples using the exact theory for various values of $k_B h$, selecting appropriate values for ϵ/ϵ_* . In this way we have examined several values of $k_B h$, taking $N = 16$, $\alpha = \pi/2$, $\beta = 32\pi/127$: see table 2. These are variants of the last example cited in table 1, which gives the ratio of the surface amplitude of nearly 9 at $\epsilon/\epsilon_* \simeq 0.3$ and $k_B h = 0.5$. Evidently it is still possible to get significant differences in the amplitude at the right and left ends even with the more accessible tank aspect ratios h/L of about 0.03 or 0.04 ($k_B h = 1.5$ or 2.0).

If $\alpha = -\beta$ the symmetry of the geometry indicates that an eigenfunction will also have some kind of left–right symmetry. In such cases, the amplitudes at the two ends of the tank are equal, smaller amplitudes occurring at the middle. We have computed a number of examples with $\alpha = -\beta = -\pi/6$, for $k_B h = 1.0$, $N = 16$ and $\epsilon/\epsilon_* = 0.3, 0.5, 0.7, 0.9$ (as well as some at $k_B h = 1.5$). An example of the eigenfunction surface profile is shown in figure 14, for $k_B h = 1.0$, $\epsilon/\epsilon_* = 0.7$. In some of these cases, not only mode 16, but also mode 17 lies inside the range of exponential behaviour. Some of these results are summarized in table 3. In the cases referring to mode 17, as with

$k_B h$	1.0	1.0	1.0	1.0	1.0	1.0	1.5	1.5
ϵ/ϵ_*	0.3	0.5	0.5	0.7	0.7	0.9	0.7	0.9
mode #	16	16	17	16	17	16	16	16
ω/ω_B	0.9995	1.0090	1.0252	1.0173	1.0268	1.0246	1.0005	1.0041
$\left \frac{\widehat{A}(x_0)}{\widehat{A}_{centre}} \right $	1.4136	1.8819	—	2.6632	—	3.8186	1.4187	1.5955

TABLE 3. Examples of symmetrical cases where two modes lie inside the range of exponential behaviour. $\alpha = -\beta = -\pi/6$ and $N = 16$.

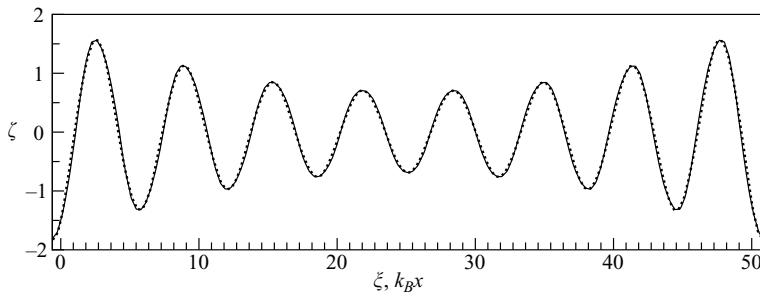


FIGURE 14. The profile of the surface elevation (at $t = 0$) from exact solutions, for $k_B h = 1.0$, $\epsilon/\epsilon_* = 0.7$, $\alpha = -\beta = -\pi/6$ and $N = 16$. —, as a function of ξ ; \cdots , as a function of $k_B x$.

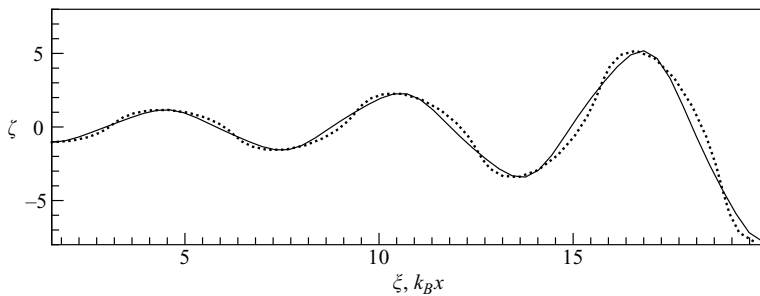


FIGURE 15. The profiles of the surface elevation (at $t = 0$) from exact solutions, for $k_B h = 0.5$, $\epsilon/\epsilon_* = 0.8038$, $\alpha = \pi/2$, $\beta = 32\pi/127$ and $N = 6$. —, as a function of ξ ; \cdots , as a function of $k_B x$. Note that this is the last example given in table 1.

any odd-numbered mode, the amplitude of the surface elevation at the centre is zero, so the end-to-centre surface amplitude ratio is not then meaningful, and has been omitted from the table.

In the examples shown in figures 12 and 14, there is little difference between ξ and $k_B x$, thus the surface profiles are almost identical whichever variable is used. This is less true when the corrugation amplitude is large and the water depth is shallow: see figure 15. Similar differences have been seen in the periodic factors of the Floquet solutions in figures 8–10.

6. Concluding remarks

We have examined the effects of regular bottom corrugations on water waves (normal modes) in a tank, using an existing asymptotic theory and by developing an exact theory which allows us to remove the restrictions on the former and to deal with the rapidly varying aspects of the flow. The exact theory has generally confirmed the accuracy of the asymptotic theory in its description of the slowly varying aspects of these waves, in particular the free surface profile near the Bragg resonance frequency ω_B . The Floquet solutions ('propagating waves') of the exact theory are *not* individually analogous to the two oppositely directed propagating waves of the flat bottom case. However, their set of linear combinations is analogous to the set of combinations of the latter (i.e. the so-called partially standing waves). The exponential behaviour near the resonance frequency is a consequence of the interaction of the two propagating waves brought about by the bottom corrugations. The way this variation is distributed along the tank, however, is sensitively determined by the precise location of the endwalls of the tank with respect to the corrugation crests. With the inclusion of evanescent modes, even only a few, the exact solutions are able to satisfy the true boundary conditions more accurately than the asymptotic solutions. We thus expect that the evanescent waves constructed here will be of relevance for problems other than normal modes which involve a corrugated bottom, whenever the presence of some agency (like the ends) means that certain aspects of the flow are not slowly varying.

Some limitations of the theoretical results given here, for applications to natural phenomena or laboratory experiments, should be mentioned. (i) The range of the frequency in which dramatic effects are expected is not very great, so that observations may require rather careful tuning. (ii) Dissipative effects have not been accounted for, but can be of importance, in particular in small-scale laboratory experiments. (iii) Although we have not required the corrugations to be of small amplitude, we have considered only the linear wave theory. For a sufficiently large amplitude of the motion, some nonlinear effect must be expected.

We should like to dedicate this paper to the memory of D. Howell Peregrine, to whom the paper was originally submitted. His untimely death has saddened us deeply. LNH has known DHP as a friend for many years. JY had close interaction with DHP in the summer of 2005 when he was the editor of another paper of hers. During that time, she acquired high appreciation for DHP's dedication and skills as an editor and a scientist.

We should like to thank two anonymous referees whose insistence on greater succinctness and careful suggestions have helped us to improve the quality of the paper.

Appendix

A.1. Connection of solutions in § 2.3 to the normal modes of a flat-bottomed tank

Since T and Ω have the same sign, as $\epsilon \rightarrow 0$ (i.e. $\Omega_c \rightarrow 0$ and $Q \rightarrow \Omega$), we have $T \rightarrow \infty$ if $\Omega > 0$ or $T \rightarrow 0^-$ if $\Omega < 0$.

Case (i): As $T \rightarrow \infty$, $\gamma_1 \rightarrow 0$ and $\gamma_2 \rightarrow 0$. From (2.20), $q = m\pi + \alpha - \beta$. Since $q > 0$, m should be non-negative, and $m = 0$ only if $\alpha > \beta$. Using (2.22), and noting that $q = \Omega L / C_g$, the surface elevation is written from (2.2) as

$$\zeta = a \cos [k_n(x_0 - x) - k_B x_0] e^{-i\omega_n t} + \text{c.c.}, \quad (\text{A } 1)$$

where $\omega_n = \omega_B + \Omega$ and $k_n = k_B + \Omega/C_g$. Taylor expansion of $\omega_n^2 = gk_n \tanh k_n h$ for small $(k_n - k_B)$ gives $\omega_n - \omega_B = (k_n - k_B) C_g$, meaning that (A 1) is indeed a normal mode of the flat-bottomed tank. Since $k_n L = k_B L + q = (N + m)\pi$, it is clear that as $\epsilon \rightarrow 0$, the mode associated with $m = 0$ connects to the N th mode of the flat-bottomed channel when $\alpha > \beta$, and for $1 \leq m \ll N$ it connects to the $(N + m)$ th mode.

Case (ii): Since $T \rightarrow 0^-$ as $\epsilon \rightarrow 0^+$, we should first set $a = Ta_1$ so that \hat{A} and \hat{B} in (2.22) survive in the limit. As in Case (i), we have $\omega_n = \omega_B + \Omega$, but $k_n = k_B - \Omega/C_g$. From (2.20), $q = m\pi + \beta - \alpha$, thus $k_n L = k_B L - q = (N - m)\pi$. As $\epsilon \rightarrow 0$, the mode associated with $m = 0$ connects to the N th mode, provided $\beta > \alpha$, and $1 \leq m \ll N$ now corresponds to the $(N - m)$ th mode.

A.2. Computation of the continued fractions

The calculation of the continued fractions is done by sequentially calculating the numerators and denominators of the convergents via the formulas as follows. These differ slightly from the formulas in the usual method due to the negative signs in (3.17).

For $M = 0$ do

$$n_1 = 1; \quad d_1 = L_n; \quad q_1 = n_1/d_1; \quad n_2 = L_{n+2}; \quad d_2 = L_n L_{n+2} - 1; \quad q_2 = n_2/d_2;$$

While $(|q_2 - q_1| > TOL)$ do $M = M + 2$;

$$n_3 = n_2 L_{n+M+2} - n_1; \quad d_3 = d_2 L_{n+M+2} - d_1; \quad q_3 = n_3/d_3;$$

$$n_1 = n_2; \quad d_1 = d_2; \quad q_1 = q_2; \quad n_2 = n_3; \quad d_2 = d_3; \quad q_2 = q_3$$

enddo; $CF_n(\mu) = q_3$.

In this bit of pseudo-code, TOL is a suitable small tolerance, chosen on the basis of the accuracy desired in the computation. It is easy to show inductively from these formulas that at any stage in the iteration we always have $q_2 - q_1 = 1/(d_2 d_1)$, so the convergence is rapid as the the denominators increase markedly.

A.3. Markley's algorithm

Given e and M , Markley's algorithm for solving Kepler's equation consists of a starting formula followed by one step of a highly accurate iterative refinement. All details are to be found in Markley (1996), but we sketch here the starting formula, whose maximum relative error, 3×10^{-4} , is already accurate enough for our purpose. This formula is based on a Padé approximation to $\sin E$, assuming $|E| \leq \pi$ and $|M| \leq \pi$, and quoted as follows:

$$A = [3\pi^2 + 1.6\pi(\pi - |M|)/(1 + e)]/(\pi^2 - 6), \quad d = 3(1 - e) + Ae,$$

$$r = 3Ad(d - 1 + e)M + M^3, \quad q = 2Ad(1 - e) - M^2, \quad w = (|r| + \sqrt{q^3 + r^2})^{2/3}$$

$$E_1 = \frac{1}{d}(2rw(w^2 + wq + q^2)^{-1} + M).$$

E_1 is the first approximation to the solution $E = E(e, M)$.

In our application, $e = \epsilon/\epsilon_*$ ($\cosh 2\eta/\cosh 2k_B h$). In solving (5.1a), $M = 2\alpha$. As β can sometimes approach $-\pi$ or π (see figure 2), M is assigned as follows in solving (5.1b) for ξ_1 . If $\pi/2 < \beta < \pi$, we set $\xi = (N + 1)\pi + \xi_1^+(\eta)$ (or $\xi_1(\eta) = \pi + \xi_1^+(\eta)$) and (5.1b) becomes $(\beta - \pi) = \xi_1^+ - \epsilon b \sin 2\xi_1^+ \cosh 2\eta$. We then set $M = 2(\beta - \pi)$. Similarly, if $-\pi < \beta < -\pi/2$, we set $\xi_1 = -\pi + \xi_1^-$, so that we solve $\beta + \pi = \xi_1^- - \epsilon b \sin 2\xi_1^- \cosh 2\eta$ for ξ_1^- , using $M = 2(\beta + \pi)$. After solving we can then reconstruct ξ_1 from ξ_1^\pm . Otherwise, $M = 2\beta$. The approximate value of $\xi_0(\eta)$ or $\xi_1(\eta)$ (or ξ_1^\pm) is obtained as $E_1/2$.

REFERENCES

- BAILLARD, J. A., DEVRIES, J. W., KIRBY, J. T. & GUZA, R. T. 1990 Bragg reflection breakwater: A new shore protection method? In *Proc. 22nd Intl Conference on Coastal Engineering, Delft*, pp. 757–768. ASCE.
- BAILLARD, J. A., DEVRIES, J. W. & KIRBY, J. T. 1992 Considerations in using Bragg reflection for storm erosion protection. *J. Waterway Port Coastal Ocean Engng* **118**, 62–74.
- BENJAMIN, T. B., BOCZAR-KARAKIEWICZ, B. & PRITCHARD, W. G. 1987 Reflection of water waves in a channel with a corrugated bed. *J. Fluid Mech.* **185**, 249–274.
- COLWELL, P. 1993 *Solving Kepler's Equation Over Three Centuries*. Willmann-Bell.
- LAMB, H. 1932 *Hydrodynamics*, 6th edn. Cambridge University Press.
- MARKLEY, F. L. 1996 Kepler equation solver. *Celest. Mech. Dynam. Astron.* **63**, 101–111.
- MEI, C. C. 1985 Resonant reflection of surface waves by periodic sandbars. *J. Fluid Mech.* **152**, 315–337.
- MEI, C. C., HARA, T. & YU, J. 2001 Longshore bars and Bragg resonance. Chapter 20 in *Geomorphological Fluid Dynamics* (ed. N. Balmforth & A. Provenzale). Lecture Notes in Physics, vol. 582. Springer.
- STRUIK, D. J. 1991 *Yankee Science in the Making*. Dover (reprint of revised edition published by Collier Books, New York, 1962).
- YU, J. & MEI, C. C. 2000a Do longshore bars shelter the shore? *J. Fluid Mech.* **404**, 251–270.
- YU, J. & MEI, C. C. 2000b Formation of sand bars under surface waves. *J. Fluid Mech.* **416**, 315–348.